ELSEVIER

Interannual variability of Martian dust storms in assimilation of several years of Mars global surveyor observations

Luca Montabone *, Stephen R. Lewis, Peter L. Read

Atmospheric, Oceanic and Planetary Physics, Department of Physics, University of Oxford, Clarendon Laboratory, Parks Road, Oxford OX1 3PU, United Kingdom

Abstract

We study the interannual variability of dust storms on Mars in an assimilation of thermal profiles and dust opacity observations into a general circulation model for the Martian atmosphere. The observations have been provided by the thermal emission spectrometer aboard the Mars Global Surveyor spacecraft during the scientific mapping phase over more than two complete Martian years, which include three dusty seasons in southern spring. A comparison between dust seasons which are characterized only by regional storms and the global, planet-encircling dust storm of 2001 is performed, focusing on the meteorological conditions which can trigger the onset and development of the global storm, and its effects on the global circulation.
© 2005 COSPAR. Published by Elsevier Ltd. All rights reserved.

Keywords: Mars; Atmosphere; Dust storms; Interannual variability; Data assimilation

1. Introduction

Dust is a fundamental component of the atmosphere on Mars and the dust heating through absorption of visible radiation has a strong impact on its thermal and dynamical state. Atmospheric variability is strongly influenced by the dust cycle and any model of the Martian atmospheric circulation needs a good representation of the seasonal variability of dust loading.

The dust cycle and storm occurrence on Mars, described by, e.g., Martin and Zurek (1993), McKim (1996), show an interannual variability which in some years manifests itself as dramatic, planet-encircling dust storms. These latter affect the thermal and dynamical structure of the lower atmosphere for long times (∼60 sols) compared to dust seasons in southern spring which

are characterized only by local and regional storms. Attempts to model this interannual variability of the dust cycle on Mars have recently been made by Newman et al. (2002a) and Basu et al. (2004), by developing a dust transport scheme for a general circulation model which enables the lifting, transport and deposition of radiatively active dust, i.e., dust which produces effects in the radiative transfer scheme. Two mechanisms for lifting are considered: lifting by near-surface wind stress and by convective vortices (known as dust devils). Although realistic annual and interannual behaviours were achieved by such parameterizations, global storms and the full range of variability are still difficult to simulate (Newman et al., 2002b).

A new approach to the study of the Martian atmosphere has been made possible by the availability of large amounts of spacecraft observations with good spatial and temporal coverage. Such an extensive atmospheric data set, mostly originating from the thermal emission spectrometer (TES, see e.g., Conrath et al., 2000; Smith et al., 2000) aboard the Mars Global

* Corresponding author. Tel.: +44 0 1865 272902; fax: +44 0 1865 272923.
  E-mail addresses: montabone@atm.ox.ac.uk, l.montabone1@physics.ox.ac.uk (L. Montabone).

Surveyor (MGS), has been shown to be suitable for data assimilation techniques in the same way as they are implemented for weather forecasting on the Earth (Lewis and Read, 1995; Lewis et al., 1996, 1997; Zhang et al., 2001). Data assimilation, in fact, provides a complete, balanced, four-dimensional best-fit to observations for all the atmospheric variables, including those for which no direct measurements are available, such as wind and surface pressure. It has already been successfully adopted by Lewis and Barker (2005) to infer some aspects of the Martian tides.

We assimilated more than two complete Martian years of atmospheric temperature profiles and dust opacities below about 40 km altitude into a general circulation model of the atmosphere, the Oxford version of the AOPP/LMD MGCM (Forget et al., 1999). The data were provided by TES in nadir mode during the MGS mapping phase which began in April 1999 and is still ongoing. This multiannual, four-dimensional (4D) picture of the Martian meteorology, which includes the global dust storm of 2001, is a unique opportunity to study the interannual variability of the dust cycle and dust storms, and their effects on the global circulation. Differences between a dust season characterized only by local or regional storms and a global dust storm season may help to give insight into the conditions which trigger the onset of a planet-encircling dust storm.

In this paper, we analyze the variability of dust storms on Mars over three dust seasons in Martian years (MY) 24–26.[1] We compare the occurrence of storms in the three seasons and analyze the meteorological conditions which differentiate them, focusing in particular on differences in near-surface wind stress, surface to air temperature difference and thermodynamic efficiency, which are the variables that can play a significant role in dust lifting. The effects of the global dust storm on the circulation are also highlighted. Although it would be desirable to find a definitive solution to the problem of which conditions determined the explosive growth of the 2001 dust storm, this is beyond the scope of this paper, and further, more detailed analyses have to be performed before getting close to a conclusive answer. The aim of this paper is, however, to show that data assimilation can definitely help to make further steps in this direction.

2. Method: data assimilation

The data assimilation in this study is conducted using a modified form of the sequential Analysis Correction

[1] In this convention, Martian year 1 begins at $L_s = 0$ on 11 April 1955; MY 24 begins on 14 July 1998. Clancy et al. (2000) propose this nomenclature as the new period of careful and 'unified' observations on Mars which begins after the observations of the global dust storm in 1956.

scheme (Lorenc et al., 1991) with parameters tuned for the specific case of Mars. Although details of this assimilation technique are given by Lewis et al. (1996, 1997, 2005) and Lewis and Barker (2005), we mention here that it combines information from both present and past observations of TES thermal profiles and dust optical depth using a GCM to produce a time-evolving analysis of the atmospheric state. Observations are repeatedly introduced to the model spread over a 6 h time window and an empirically determined horizontal correlation scale (∼340–540 km), both weighted towards the actual observation time and location, in order to adjust the large-scale and slowly varying components of the atmospheric flow.

It is worth mentioning here that dust opacity is measured by TES at $1075 \, \text{cm}^{-1}$ in the infrared, so the TES opacities are doubled as a conversion to the GCM broadband visible opacity. Conversion factors in the range 1.5–2.5 have not shown any significant difference in the results of the assimilation. The nadir observations, furthermore, do not provide any information about the vertical distribution of dust in the lower atmosphere, and only total opacity from ground to space can be assimilated. The vertical distribution of the dust volume mixing ratio at a given latitude, longitude and time in the model has therefore to be prescribed by an analytical equation of the form

$$q = q_0 \exp\left\{a\left[1 - (p_0/p)^{(b/z_{\max})}\right]\right\} \qquad (1)$$

for pressure $p \leqslant p_0$, where p_0 is taken to be $p_0 = 700$ Pa, and with $q = q_0$ for $p > p_0$ (Forget et al., 1999). q_0 is calculated to give the assimilated total (visible) opacity at the appropriate latitude and longitude, and a and b are free parameters with values $a = 0.007$, $b = 70$ km. $z_{\max}$ (the "top" of the dust layer) varies with areocentric longitude L_s and latitude ϕ according to the equation

$$z_{\max} = 60 + 18\sin(L_s - 160°) - \sin^4\phi[32 \\ + 18\sin(L_s - 160°) - 8\sin(L_s - 160°)\sin\phi]. \quad (2)$$

This dust distribution seems to give a reasonable statistical match to observations when used in the GCM (Forget et al., 2001). Because of the lack of information about the vertical distribution of dust, for the purposes of this paper the GCM was not allowed to transport dust actively, although this remains an objective for future work (see also Section 5).

The assimilation we performed spans from $L_s = 141°$ (middle northern hemisphere summer) in MY 24 to $L_s = 250°$ (late northern hemisphere autumn) in MY 26, including the global dust storm in MY 25. The distribution of dust observations in latitude and time during this period is shown in Fig. 1. Since there is a lack of dust observations at high latitudes during the dust seasons in southern spring, we will focus in this work on latitudes between 40°N and 60°S. This is not a significant
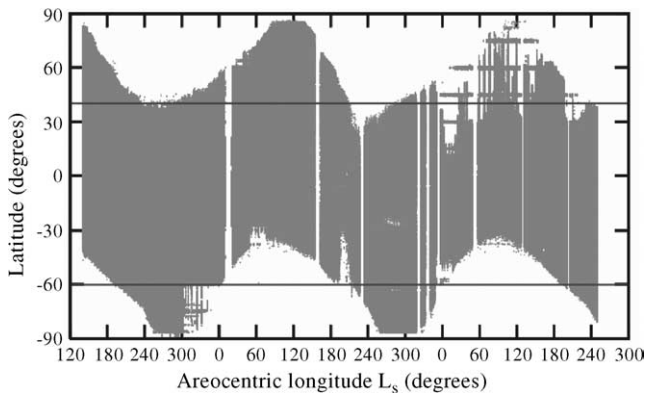
Fig. 1. Distribution in latitude and time of assimilated dust observations from TES. The two straight lines bound the latitude band we focus on: 40°N–60°S. The lack of dust observations at high latitudes in autumn/winter/early spring is due to the reduced thermal contrast between the atmosphere and the ground, covered by CO_2 ice.

limitation because most of the big dust storms occur in this latitude band.

3. Interannual variability of dust storms

Fig. 2 shows the time and latitude variations of the zonal average of the equivalent dust optical depth, normalized to the reference pressure of 700 Pa to remove topographic effects. This figure illustrates the overall variability of dust loading into the atmosphere over the three observed dust seasons, highlighting the extreme nature of the season in MY 25 with respect to the other two. Features with repeatable seasonal and spatial characteristics in all three Martian years (where observations are available) are an early peak (around $L_s = 180°$) of dust opacity limited to a narrow latitude band centered around 50°S, a late peak more spread in latitude around $L_s = 340°$ and high values of the optical depth at high southern latitudes, shifted later in time with respect to the main peak (likely due to dust reservoirs which become available after the withdrawal of the southern ice cover). The dust season in MY 25 shows both an increase in dust
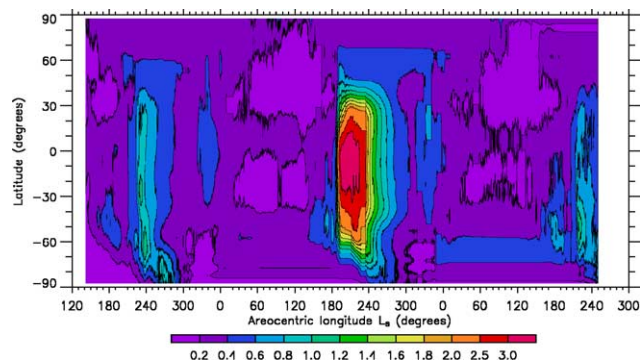

Fig. 2. Zonal average of equivalent total visible dust opacity normalized at the reference pressure of 700 Pa.

opacity of about three times more than the other seasons and an earlier and more rapid growth. The overall opacity starts to increase monotonically at $L_s \sim 185°$ at a rate of about 0.14 per sol until $L_s \sim 195°$ (on average, over a latitude band 40°N–60°S. See also Fig. 4, upper panel), reaches its maximum at $L_s \sim 214°$, then decreases slowly over a range of more than 100° of areocentric longitude. For comparison, in the previous year the opacity started to increase at a rate of about 0.004 per sol after $L_s \sim 212°$, and more substantially at a rate of about 0.03 per sol after $L_s \sim 222°$. In MY 26, the opacity increased at a rate of about 0.01 per sol after $L_s \sim 207°$ and 0.05 after $L_s \sim 214°$. Although an abrupt increase in dust loading is a common feature of all three MGS-observed Martian years, as well as of all the other well-observed years from ground-based or previous spacecraft observations, the rate and the time of the year this increase occurred make MY 25 unique among the other MGS-observed years.

The localization of the major dust storms which raise the overall dust loading in the atmosphere (due to the advection of the lifted dust) also varies with season, as shown in Fig. 3. In MY 24, two regional dust storms developed in the Chryse region (at $L_s \sim 210°$ and $L_s \sim 222°$) and in the Amazonis region ($L_s \sim 226°$), whereas in MY 25 the global dust storm started as a regional storm between Hellas and Isidis Planitia and rapidly grew to planetary scale thanks to the eastward migration and the consequent contribution of dust from the Tharsis region and the plains south of the Tharsis ridge.[2] This may be due to a positive feedback of the dust cloud which strengthens the near-surface wind stress, which in turn enhances the lifting of more dust (Newman et al., 2002a). MY 26 also exhibited a regional dust storm developing between Hellas and Isidis Planitia, although later than the previous year, but this did not grow sufficiently to produce a global storm, and faded out after only 12 sols.

4. Dust storms and meteorology

The onset and early development of dust storms are connected to the intensity of surface winds, which can be local (e.g., the anabatic and katabatic winds around the Tharsis peaks and Hellas basin, driven by the horizontal temperature gradients resulting from heating over slopes) or, more generally, a result of the global circulation (e.g., the strong westerly winds at about 30°S in southern summer, a result of the existence of the rising branch of a single, cross-equatorial Hadley cell at that time of the year and at that latitude, outside any planet-encircling storm which, on the contrary, would

---

[2] Cfr. images from the Mars Orbiter Camera aboard MGS, which are available, for instance, on http://www.msss.com/mars_images/moc/10_11_01_dust_storm/.
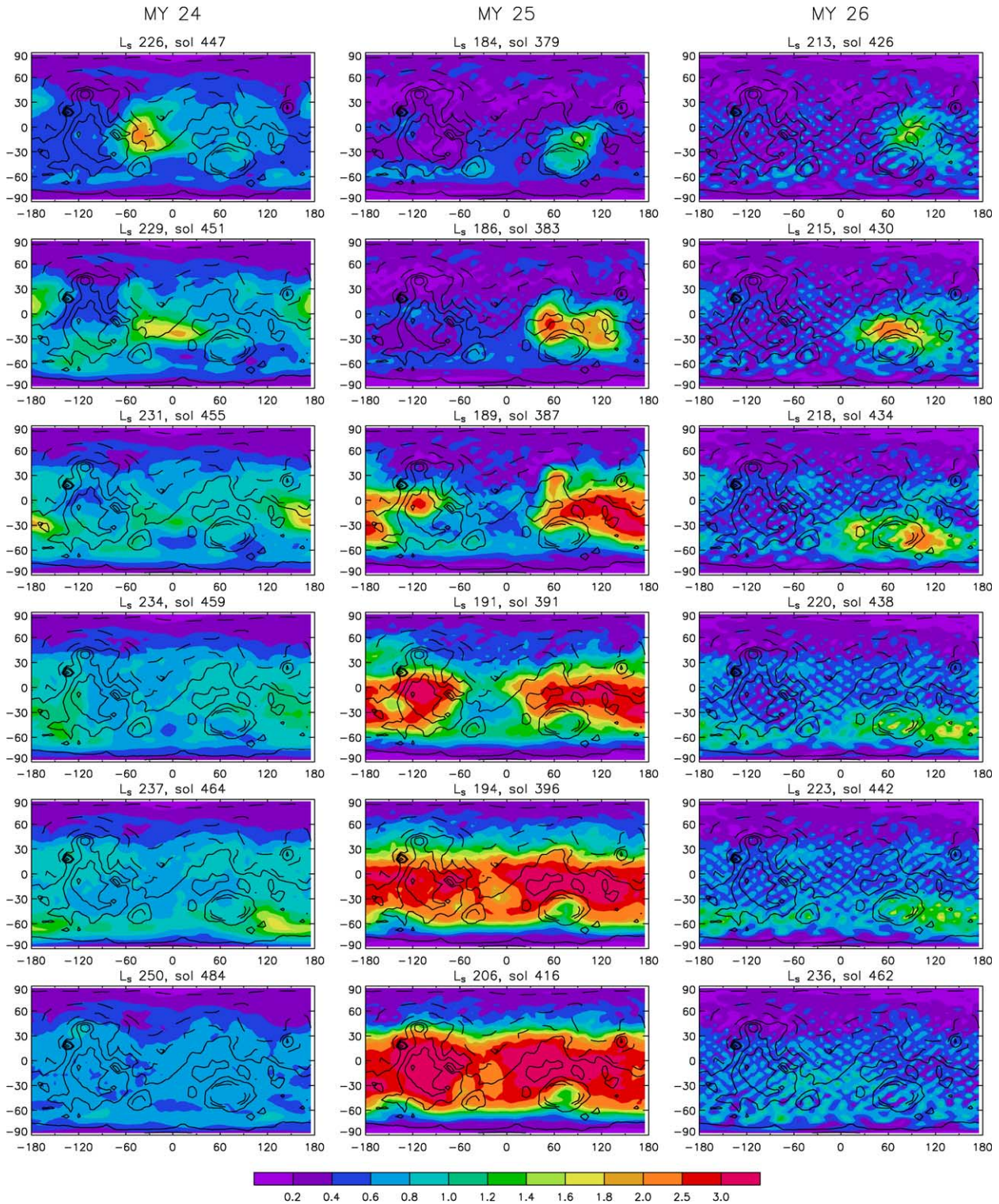
Fig. 3. Evolution of dust storms in MY 24–26. All the snapshots show the latitude–longitude distribution of the dust total optical depth normalized to 700 Pa. Note the dramatic time scale of the growth of the regional storm between Hellas and Isidis Planitia up to planetary scale in MY 25: it only took 18 sols to encircle the entire planet with an average dust loading three times larger than that in the other two years.

strongly modify the meridional circulation). Since the global circulation patterns have little intrinsic interannual variability (see e.g., Newman et al., 2004), the variability of dust storm occurrence is therefore determined mostly by the interannual variability of the local meteorology, enhanced or reduced by a number of positive or negative feedbacks. Established dust storms, however, can have a big impact on the large scale variability.

The possibility of dust devils triggering the onset of local dust storms should also be considered, since the amount of dust lifted by these atmospheric vortices can be considerable. Their strength, and therefore their capability to lift more dust, is determined by surface to air temperature difference and thermodynamic efficiency. Nevertheless, Newman et al. (2002a) noted that a negative feedback is produced and less dust is lifted by dust devils as the atmospheric dust load increases.

In order to characterize and try to explain the interannual variability of the onset of dust storms, it is therefore useful to analyze the meteorological variables which can be somehow related to the process of dust lifting, namely the near-surface wind stress (which depends on the wind speed), the surface to air temperature difference and the thermodynamic efficiency. According to Newman et al. (2002a, 2005), a model of dust lifting by near-surface wind stress predicts that the vertical flux of lifted dust, V_N is proportional to the horizontal saltation flux of sand

$$V_N \propto \frac{1}{\sqrt{\rho}} \left(\zeta^{3/2} + \zeta \zeta_t^{1/2} - \zeta^{1/2} \zeta_t - \zeta_t^{3/2} \right), \tag{3}$$

where ρ is the near-surface air density, ζ is the near-surface wind stress magnitude and ζ_t is an empirically determined stress threshold for the lifting to occur. The wind stress is related to the near-surface wind speed, U through the equation

$$\zeta = \rho \left(\frac{kU(z)}{\ln(z/z_0)} \right)^2, \tag{4}$$

where k is von Kármán's constant (here, $k = 0.4$), z is height above the surface (here, $z = 4.6$ m, the average height of the lowest layer in the model) and z_0 is the height at which velocities go to zero (roughness height, taken as 0.01 m). The flux of dust lifted by the activity of dust devils can be modeled by taking into account the heat input to the base of the vortex (which increases with surface to air temperature difference) and the fraction of the input heat which is turned into work, which is the thermodynamic efficiency, increasing with the depth of the convective boundary layer:

$$\eta \equiv 1 - \frac{p_s^{\chi+1} - p_{top}^{\chi+1}}{(p_s - p_{top})(\chi+1)p_s^{\chi}}, \tag{5}$$

where p_s is the surface pressure, p_{top} is the pressure at the top of the convective boundary layer (defined in the model as the pressure at which the turbulent kinetic energy falls below a critical value of 0.5 m^2 s^{-2}), and χ is the specific gas constant divided by the specific heat capacity at constant pressure. The surface to air temperature difference determines the energy available to drive any dust devil which may form, whereas the thermodynamic efficiency relates to how high (and hence how large and strong) dust devils are able to grow.

In this section, we analyze the interannual variability of these variables, in order to assess the relative importance of these two models of dust lifting in relation to the onset of the dust storms, in particular the 2001 global storm. Fig. 4 demonstrates that the interannual variability of surface winds correlates very well in time with the variability of dust optical depth. This picture plots the average of near-surface wind speed and wind stress over the latitude band 40°N–60°S, smoothed by a 1-sol running mean, and compares them to the zonal mean of dust optical depth at 700 Pa averaged over the same latitude band. The comparison highlights that, on average, the dramatic increase in optical depth at $L_s \sim 185°$ in MY 25 matches perfectly with the steep increase both in the magnitude of surface wind which, over 5° of areocentric longitude (about 8 sols), becomes about 35% larger than the other two years at the same time, and in the surface wind stress. Such an increase of surface wind magnitude with respect, for instance, to the previous year is at first concentrated around the northern and eastern slopes of Hellas basin (high slope winds), then extends to the Tharsis ridge, the Syria Planum and Solis Planum, south of Tharsis (see Fig. 5). Sometime after $L_s = 195°$, a narrow band of strong surface winds strengthens between 30°S and 60°S, which is in accordance with the enhancement
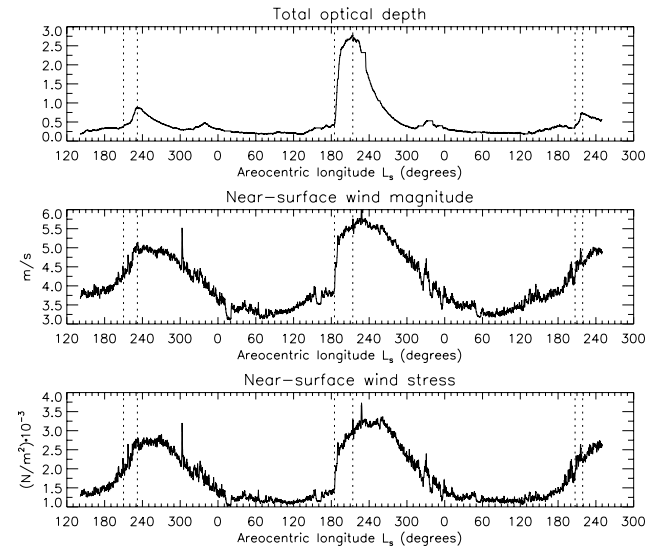

Fig. 4. The upper panel represents the average of the dust optical depth at 700 Pa over the latitude band 40°N–60°S, smoothed in time by using a 1-sol running mean. The middle panel is the average of the near-surface wind magnitude (wind speed at 4.6 m) over the same latitude band, and the lower panel is the average of the near-surface wind stress, as defined in Eq. (4). The dashed lines highlight the time intervals between the base and the maximum of the peaks of total optical depth. They correspond respectively to the intervals of areocentric longitude 210°–232° in MY 24, 185°–214° in MY 25, and 207°–219° in MY 26. The sharp spikes in wind speed and stress correspond to the passage of fast weather systems; the one in MY 24, for instance, is due to strong winds mainly concentrated in Chryse Planitia, the Tharsis region and the Amazonis Planitia over three sols around 2 p.m. local time.
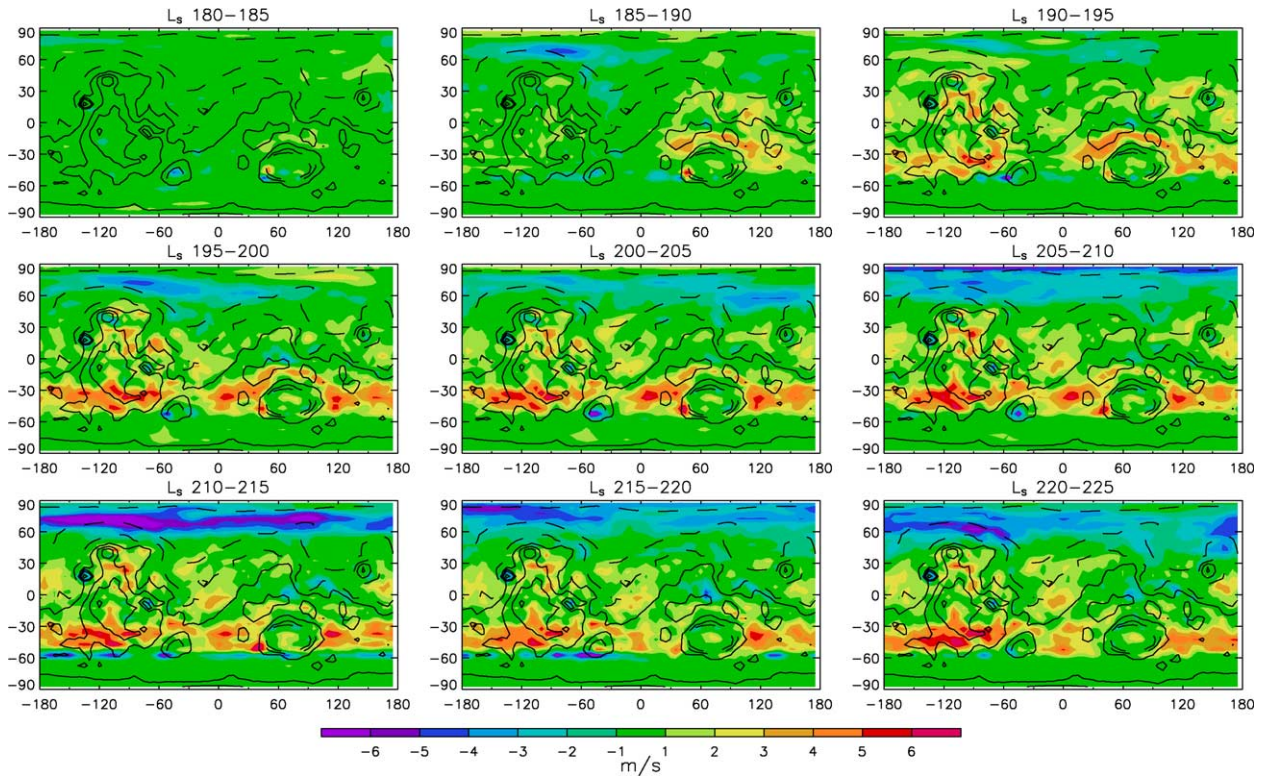
Fig. 5. These plots represent the difference of near-surface wind speed between MY 25 and MY 24, averaged over 5° of areocentric longitude, for the period L_s=180–225. Although the average is performed over all times of the day, anomalies in MY 25 appear to be significant, both during the onset and the further development of the global storm. Anomalies are even stronger if averaged at fixed times of the day, around noon local time (not shown here).

of the negative, counterclockwise Hadley circulation cell which has its ascending and descending branches centered around these latitudes (see Fig. 7).

The anomalies in surface wind speed correlate very well with anomalies in surface wind stress, as Fig. 6 shows, even where the air density is lower (e.g., the Tharsis region). According to the model of dust lifting described by Eq. (3), this in turn should increase the amount of dust which is lifted into the air, although a preliminary study without transporting dust was not
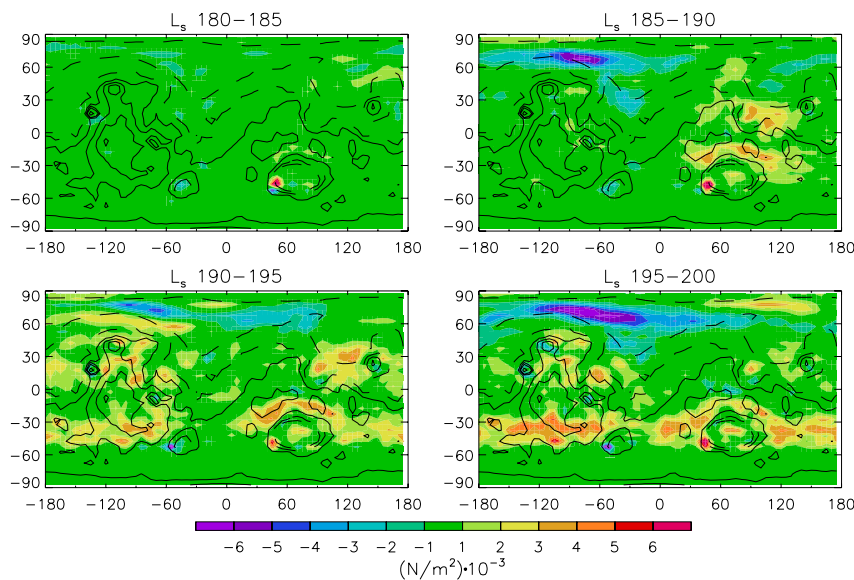

Fig. 6. Near-surface wind stress anomalies between MY 25 and MY 24, averaged over 5° of areocentric longitude, for the period L_s=180–200. These plots correlate well with the corresponding plots of surface wind speed anomalies in Fig. 5, even where air densities are lower.
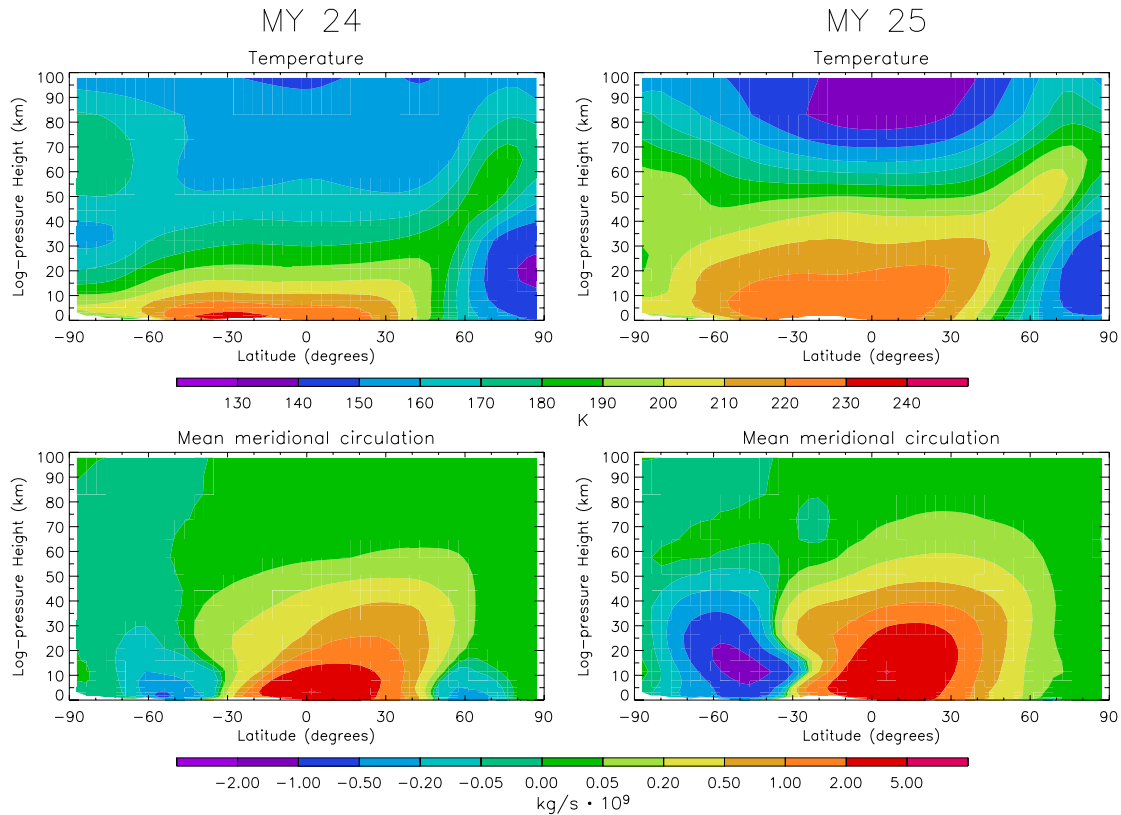
Fig. 7. Effects of the planet-encircling dust storm in MY 25 on the global circulation, in comparison with the previous Martian year. The plots show the temperature and mean meridional circulation averaged over 30° of areocentric longitude (L_s=195–225).

able to reproduce the explosive increase of observed dust optical depth in MY 25 with respect to the increase in the previous year which is shown in the upper panel of Fig. 4. Future work will address this issue in detail. Although surface wind stress anomalies between MY 25 and MY 24 correlate with wind speed anomalies even where air densities are lower, in an absolute sense wind stress remains weak, on average, when wind speed starts to increase before the onset of the three dust seasons (namely, before $L_s \sim 180°$ in all three years), as the middle and lower panels of Fig. 4 show. This is in very good agreement with the low values of total optical depth outside the dust storm peaks. Another interesting characteristic of all three years which can be observed in Fig. 4 is that the total optical depth decreases roughly exponentially after having reached the maximum, despite the fact that both the wind speed and the wind stress are at their maximum values. This is particularly evident in the case of the global storm, when the wind stress at $L_s \sim 260°$ is still at its maximum value (averaged over the latitude band), but the optical depth has decreased almost by 2/3. The decay of dust storms on Mars is a phenomenon which is not completely understood yet, and it is clear that deposition of dust by local gravitational sedimentation cannot fully explain the graphs in Fig. 4, as deposited dust should be lifted again by strong

wind stress. Nevertheless, it is important to report here that the start of the decay of the 2001 storm at $L_s \sim 214°$ coincided with the onset of the fully developed counterclockwise Hadley circulation cell between 30°S and 60°S and the strengthening of the clockwise cell between 30°S and 60°N, which could have forced some of the atmospheric dust to move southwards and northwards and deposit at very high latitudes, where wind stress is generally weaker. This hypothesis might be investigated in future by allowing the transport and deposition of dust between observations in the model.

The effects of the planet-encircling dust storm are evident not only in the change of the dynamics of the atmosphere but also in the increase of the temperature below 60 km altitude, as shown in the upper panels in Fig. 6 for the period $L_s = 195°$–225°. The temperature increase during the global dust storm (right panels) is as large as ~ 30 K at a height of 20 km above the equator. This effect is due to the increased absorption of visible radiation by the suspended dust, which in turn has the consequence of cooling the surface by more than 20 K in some locations during the day (not shown here). The combination of these two effects yields a negative feedback on the development of dust devils during dust storms, as described by Newman et al. (2002a). Fig. 8, in particular, is a plot of the difference between MY 25 and
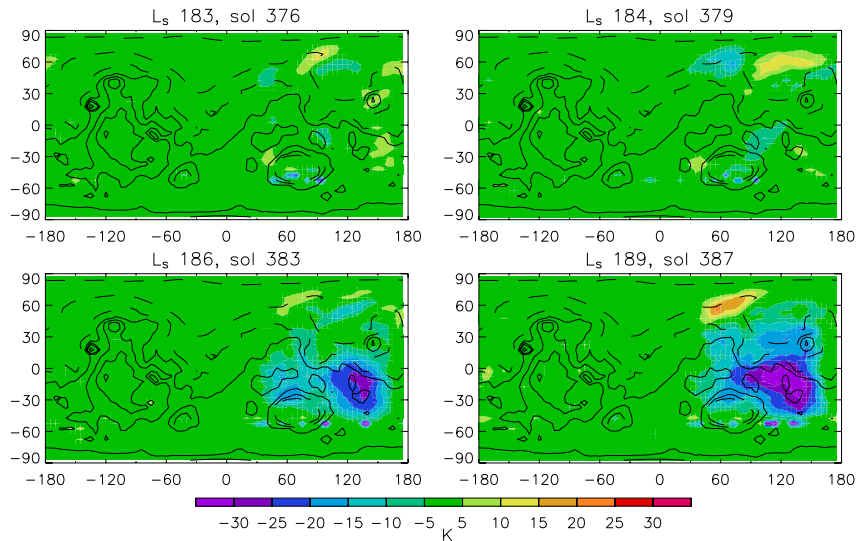
Fig. 8. Difference between MY 25 and MY 24 of the surface to air temperature difference at noon at 90°E for 4 sols before and during the development of the dust storm around Hellas which leads to the global storm in MY 25.

MY 24 of the surface to air temperature at noon at 90°E (where the initial Hellas storm formed), for four different sols. It demonstrates that this temperature difference in MY 25 decreases as soon as the dust storm develops around the northern slopes of Hellas, preventing the formation of dust devils which could sustain the development of the storm in that region. It also shows (upper panels) that there were no anomalously large surface to air temperature differences around Hellas before and during the onset of the dust storm in MY 25, at a time of the day when these differences should be large. Neither was anomalously large thermodynamic efficiency found in the sols preceding the onset of the storm in the region of Hellas (see upper panels of Fig. 9), although the presence of dust in the atmosphere subsequently raises the top of the convective boundary layer, thus increasing the available thermodynamic efficiency. Nevertheless, the lack of anomalies both in the surface to air temperature difference and thermodynamic efficiency before the onset of the 2001 storm in Hellas indicates that most likely the role of dust devils in triggering such a storm was marginal, if at all. Besides, the subsequent anticorrelation between these two variables suggests that even the role played by convective vortices in lifting dust during the development of the global storm was marginal with respect to the lifting of dust by near-surface wind stress, which seems to be the prevalent mechanism.
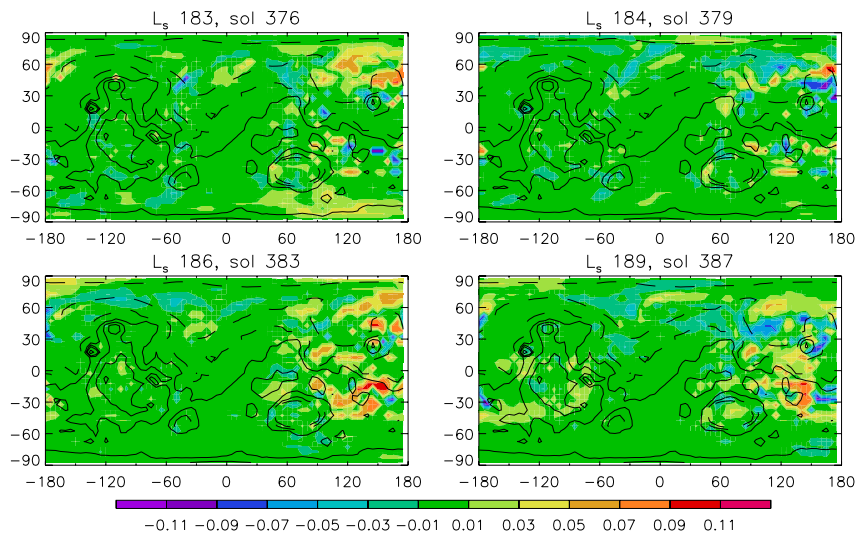

Fig. 9. Difference between MY 25 and MY 24 of the thermodynamic efficiency (as defined by Eq. (5)) at noon at 90°E for 4 sols before and during the early development of the dust storm around Hellas.

5. Conclusions

In this paper we studied the interannual variability of the dust storms during the three Martian years for which TES aboard MGS provided observations to date. We assimilated temperature profiles and dust opacities below about 40 km altitude into a general circulation model of the atmosphere. This technique provides a full set of balanced fields of variables which fit the observations and allow for an insight into the meterological conditions which trigger the onset of the dust storms, giving access to variables not directly observed. In particular, we focused on the global dust storm of 2001 (MY 25) and found that the early onset of such a storm can be linked to an anomalously large near-surface wind stress around the northern slopes of the Hellas basin, followed by large surface wind stress anomalies in the Tharsis region (Tharsis ridge, Syria Planum and Solis Planum). The large dust loading into the atmosphere had strong thermal and dynamical effects which in turn created positive feedbacks for the sustenance of the storm for several sols. On the other hand, the effect of dust lifting by dust devils has not been found to be relevant for the onset and development of this planet-encircling storm.

Three questions about the 2001 dust storm remain still open and will be addressed in future work: (1) which conditions determine the initial anomaly of near-surface wind stress around the Hellas basin, which leads to the global spread of the storm; (2) why the overall dust opacity rapidly decreases after about 50 sols despite the wind stress remaining strong; (3) which model of dust lifting by near-surface wind stress is able to reproduce the explosive character of the dust loading into the atmosphere. The answer to the first question, in particular, seems to be related to the effect of travelling waves along the southern cap edge, enhanced by the diurnal thermal tide, according to an hypothesis formulated by Gawrych et al. (2004) which arises from earlier ideas by Leovy et al. (1973).

Data assimilation has been shown to be a uniquely powerful means to study dust storms on Mars, providing reliable information about global winds and other variables not directly accessible to observations. A further application of this technique to the study of the dust cycle is to perform a complete test of the dust lifting, transport and deposition schemes on which GCMs rely, in order to assess their capability to reproduce the inter-annual variability of dust loading into the atmosphere outside any planet-encircling dust storm. This topic will be addressed in a forthcoming paper.

Future work would also take advantage of a better knowledge of the vertical structure of the dust distribution or at least of its vertical extent, which at the moment are inferred from indirect considerations of particle sedimentation and eddy mixing. The Mars Climate Sounder experiment on the 2005 Mars Reconnaissance orbiter should provide such an improvement (Taylor et al., 2005). A better knowledge of such a vertical distribution would also allow to transport dust between observations in the model without relying on analytical functions which can make this process too sensitive to the chosen parameters.

References

Basu, S., Richardson, M.I., Wilson, R.J. Simulation of the Martian dust cycle with the GFDL Mars GCM. J. Geophys. Res. 109 (E11), 2004.

Clancy, R.T., Sandor, B.J., Wolff, M.J., Christensen, P.R., Smith, M.D., Pearl, J.C., Conrath, B.J., Wilson, R.J. An intercomparison of ground-based millimeter, MGS TES, and Viking atmospheric temperature measurements: seasonal and interannual variability of temperatures and dust loading in the global Mars atmosphere. J. Geophys. Res. 105, 9553–9571, 2000.

Conrath, B.J., Pearl, J.C., Smith, M.D., Maguire, W.C., Dason, S., Kaelberer, M.S., Christensen, P.R. Mars Global Surveyor thermal emission spectrometer (TES) observations: atmospheric temperatures during aerobraking and science phasing. J. Geophys. Res. 105, 9509–9519, 2000.

Forget, F., Hourdin, F., Fournier, R., Hourdin, C., Talagrand, O., Collins, M., Lewis, S.R., Read, P.L., Hout, J.-P. Improved general circulation models of the Martian atmosphere from the surface to above 80 km. J. Geophys. Res. 104, 24,155–24,176, 1999.

Forget, F., Wanherdrick, Y., Lewis, S.R. Validation of the Mars general circulation model and climate database with new spacecraft observations. Technical Note for ESA Contract 11369/95/NL/JG, Work Package 7, 2001.

Gawrych, J., Haberle, R.M., Malin, M., Cantor, B., Smith, M.D. Analysis of the 2001 Global Dust Storm with a Mars General Circulation Model Bulletin of the American Astronomical Society, 36 #4, 2004.

Leovy, C.B., Zurek, R.W., Pollack, J.B. Mechanisms for Mars dust storms. J. Atmos. Sci. 30, 749–762, 1973.

Lewis, S.R., Read, P.L. An operational data assimilation scheme for the Martian atmosphere. Adv. Space Res 16 (6), 9–13, 1995.

Lewis, S.R., Collins, M., Read, P.L. Martian atmospheric data assimilation with a simplified general circulation model: orbiter and lander networks. Planet. Space Sci. 44, 1395–1409, 1996.

Lewis, S.R., Collins, M., Read, P.L. Data assimilation with a Martian atmospheric GCM: an example using thermal data. Adv. Space Res. 19 (8), 1267–1270, 1997.

Lewis, S.R., Barker, P.R. Atmospheric tides in a Mars general circulation model with data assimilation. Adv. Space Res. (this issue), doi:10.1016/j.asr.2005.05.122.

Lewis, S.R., Read, P.L., Conrath, B.J., Pearl, J.C., Smith, M.D. Assimilation of thermal emission spectrometer atmospheric data during the Mars Global Surveyor aerobraking period. Icarus (submitted).

Lorenc, A.C., Bell, R.S., Macpherson, B. The Meteorological Office analysis correction data assimilation scheme. Quart. J. Roy. Meteor. Soc. 117, 59–89, 1991.

Martin, L.J., Zurek, R.W. An analysis of the history of dust activity on Mars. J. Geophys. Res. 98, 3221–3246, 1993.

McKim, R.J. The dust storms of Mars. J. Br. Astron. Assoc. 106, 185–200, 1996.

Newman, C.E., Lewis, S.R., Read, P.L., Forget, F. Modeling the Martian dust 1. Representations of dust transport processes. J. Geophys. Res. 107 (E12), 5123, doi:10.1029/2002JE001910, 2002a.

Newman, C.E., Lewis, S.R., Read, P.L., Forget, F. Modeling the Martian dust 2. Multiannual radiatively active dust transport simulations. J. Geophys. Res. 107 (E12), 5124, doi:10.1029/2002JE001920, 2002b.

Newman, C.E., Read, P.L., Lewis, S.R. Investigating atmospheric predictability on Mars using breeding vectors in a general circulation model. Quart. J. Roy. Meteorol. Soc. 130 (603), 2971–2989, 2004.

Newman, C.E., Lewis, S.R., Read, P.L. The atmospheric circulation and dust activity in different orbital epochs on Mars. Icarus 174, 135–160, 2005.

Smith, M.D., Pearl, J.C., Conrath, B.J., Christensen, P.R. Mars Global Surveyor thermal emission spectrometer (TES) observations of dust opacity during aerobraking and science phasing. J. Geophys. Res. 105, 9539–9552, 2000.

Taylor, F.M., Calcutt, S.B., Read, P.L., Lewis, S.R., McCleese, D.J., Schofield, J.T., Zurek, R.W. Atmospheric temperature sounding on Mars, and the climate sounder on the 2005 Reconnaissance orbiter. Adv. Space Res. (this issue), doi:10.1016/j.asr.2005.03.072.

Zhang, K.Q., Ingersoll, A.P., Kass, D.M., Pearl, J.C., Smith, M.D., Conrath, B.J., Haberle, R.M. Assimilation of Mars Global Surveyor atmospheric temperature data into a general circulation model. J. Geophys. Res. 106, 32863–32877, 2001.